THE ASTROPHYSICAL JOURNAL, 883:91 (15pp), 2019 September 20 https://doi.org/10.3847/1538-4357/ab3c4e

On the Relation between Flare and CME during GLE-SEP and Non-GLE-SEP Events

K. A. Firoz[1,2], W. Q. Gan[2], Y.-J. Moon[1], J. Rodríguez-Pacheco[3], and Y. P. Li[2]
[1] School of Space Research, Kyung Hee University, Yongin-si, Gyeonggi-do, 17104, Republic of Korea
[2] Key Laboratory of Dark Matter and Space Astronomy, Purple Mountain Observatory, Chinese Academy of Sciences, 210008 Nanjing, People's Republic of China
[3] Space Research Group, Alcalá University, E-28871 Alcalá de Henares, Spain
Received 2019 June 29; accepted 2019 August 16; published 2019 September 24

Abstract

Association of solar flares and coronal mass ejections (CMEs) with ground-level enhancement (GLE) is a recognized fact, but questions arise when a similar association is observed for non-GLEs. In this respect, we carry out a detailed study of the relation between flare fluences (ϕ J m^{-2}) and CME speeds ($V_{\rm cme}$ km s^{-1}) during some selected GLEs and non-GLEs. As we found, most of the data points of ϕ (J m^{-2}) and $V_{\rm cme}$ (km s^{-1}) of GLEs follow a near-linear trend, with the ϕ (J m^{-2}) increasing as the $V_{\rm cme}$ (km s^{-1}) increases, resulting in a strong positive correlation ($r \geqslant 0.82$), while the correlation ($r \leqslant 0.47$) remains weak for non-GLEs. For any exceptional GLE, the ϕ (J m^{-2}) and $V_{\rm cme}$ (km s^{-1}) that do not maintain a near-linear trend over the whole flare phase do maintain at least a minimum rational proportionality over the flare rise phase, whereas this characteristic was not generally observed for non-GLEs. Although the ϕ (J m^{-2}) and $V_{\rm cme}$ (km s^{-1}) of some non-GLEs show a trend similar to those of GLEs, they indeed originated over the flare impulsive phases concomitant with coronal shock manifested in m type II bursts, while GLEs originated over the flare initial phase before the m type II. Flare peak fluences ($\phi_{\rm pk}$ J m^{-2}) and $V_{\rm cme}$ (km s^{-1}) maintain weak correlation for both GLEs and non-GLEs, likely because the CME main acceleration ceases around the flare peak. However, though the $\phi_{\rm pk}$ (J m^{-2}) governs the flare total fluence, it does not blur the correlation between the fluence over the flare rise phase (ϕ_r J m^{-2}) and $V_{\rm cme}$ (km s^{-1}), indicating that the flare peak/strength does not control the GLE occurrence.

Unified Astronomy Thesaurus concepts: The Sun (1693)

1. Introduction

Ground-level enhancement (GLE) appears in the cosmic-ray temporal profile conspicuously as a sudden, sharp, and short-lived increase with sufficient intensity rising above the galactic cosmic-ray background. While the energetic particle fluxes comprise softer and harder spectra, the softer phase representing MeV energetic particle fluxes refers to the solar energetic particle (SEP) event, and the harder phase representing GeV energetic particle fluxes refers to the GLE event. Thus, the GLEs are recognized as the relativistic extension of SEPs, and the GLE (GeV) events consistently represent the most energetic class of SEPs (MeV). Details can be studied in the literature (e.g., Smart et al. 1971; Cliver et al. 1982, 1983; Fujimoto et al. 1985; Shea et al. 1987; Debrunner et al. 1990; Baisultanova et al. 1991; Nagashima et al. 1992; Duldig et al. 1993; Vashenyuk et al. 1993, 2003, 2011; Kahler 1994; Kudela et al. 1995; Shea & Smart 1996; Cramp et al. 1997; Lovell et al. 1998; Duldig 1999; Clem & Dorman 2000; Duldig 2001; Deeley et al. 2002; Bieber et al. 2004, 2013; Belov et al. 2005, 2015; Pérez-Peraza et al. 2006, 2018; Plainaki et al. 2007; Bazilevskaya 2008; Bütikofer et al. 2009; Mewaldt et al. 2012; Kurt et al. 2010; Vashenyuk et al. 2011; Maurchev et al. 2013; Velinov & Mishev 2013; Gopalswamy et al. 2014; Papaioannou et al. 2014; Pérez-Peraza & Juárez-Zuñiga 2015; Grechnev & Kochanov 2016; Asvestari et al. 2017; Belov & Struminsky 2017; Raukunen et al. 2018).

Solar flares and coronal mass ejections (CMEs) are the particle acceleration processes that can accelerate particles to relativistic energies, and thus the SEP (MeV) particles can be accelerated to GLE (GeV) particles. The particles accelerated by the acceleration processes travel through the interplanetary magnetic field medium and intrude sporadically into the atmosphere. They undergo collisions with atoms of the upper atmosphere, generate cascades, and shower down onto the surface of the Earth. Due to the steep energy spectrum of the MeV particles, at times only a small fraction accelerated to the energy of $\geqslant$1 GeV generates cascades in the atmosphere sufficiently, thereafter appearing as GLEs in the cosmic-ray intensity profile registered by neutron monitors on the Earth (e.g., Shea & Smart 1982; Kudela 1990; Kudela et al. 1993; Vashenyuk et al. 1994, 1997; Kudela & Langer 1995; Belov & Eroshenko 1996; Reames 1999; Sabbah 2000; Hofer & Storini 2001; El-Borie 2003; Plainaki et al. 2005; Saiz et al. 2005; Mavromichalaki et al. 2006, 2007; Grechnev et al. 2008; Andriopoulou et al. 2009, 2011a, 2011b; Papaioannou et al. 2009, 2014, 2016; Firoz et al. 2010, 2012, 2014a; Aschwanden 2012; Grechnev et al. 2013; Miroshnichenko et al. 2013; Kühl et al. 2015; Dierckxsens et al. 2015; Mishev & Usoskin 2016; Mishev et al. 2017, 2018; Wu & Qin 2017; Heber et al. 2018).

The SEPs are the dominant source of ionization in Earth's upper atmosphere and a major source of natural radiation on the Earth's surface. The magnitude of the SEP flux intensity increase specifies the enhancement of the radiation level, which can cause damage to satellite electronics and also pose a radiation hazard to astronauts and air crews (e.g., Kuwabara et al. 2006; Mavromichalaki et al. 2007; Hu et al. 2009; Shea & Smart 2012; Mironova et al. 2015; Grechnev et al. 2017). Owing to the huge difference in energy level, GLE (GeV) particles arrive at the Earth much earlier than the SEP (MeV) particles (e.g., Firoz et al. 2019), and the alarm of severe weather at near-Earth space can instantly be performed on the ground by inspecting the increased radiation exposure above the background traditionally noticed in the cosmic-ray intensity profile during the GLE events (e.g., Storini et al. 2005; Vashenyuk et al. 2006; Mavromichalaki et al. 2007, 2013; Makhmutov et al. 2009; Belov et al. 2010; Firoz et al. 2011a, 2011b; Papaioannou et al. 2018). Thus, the GLE observations may enable us to be warned of the arrival of the SEP event and thereby the plight of the space weather. So, it is important to understand the mechanism of GLE events.

2. Statement of the Problem

Several researchers (e.g., Pérez-Peraza et al. 2006; Simnett 2006, 2007; Bombardieri et al. 2008; Kurt et al. 2010, 2013, 2018; Aschwanden 2012; Mewaldt et al. 2012) observed that GLEs exhibit spectra with the highest energy that represents the strongest acceleration process (i.e., flare). They further found a temporal relationship between the rise phases of flare components and growth phase of GLEs and suggested that the seed particles of GLEs might be produced by the flares. This is contrary to the suggestions of some other researchers (e.g., Reames 1999; Kahler et al. 2001; Gopalswamy et al. 2004; Kahler & Vourlidas 2005) that the GLE onset behavior can be determined by when and where the CME-driven shock develops, and a prior CME can produce seed particles that can be reaccelerated by the main CME. In corroboration with them, Gopalswamy et al. (2014) further suggested that GLEs can be produced by the CMEs depending on the latitudinal and ambient condition.

Simnett (2006, 2007) argued that if the protons are accelerated by the CMEs, then the protons are supposed to derive the energies from the CMEs, and as the CMEs traditionally develop on much wider heliolongitudes, they allow much more free energy than the flares, which are usually developed on narrower heliolongitudes. Simnett thus found that the characteristics of the protons are inconsistent with CME-shock acceleration while consistent with the flare acceleration process. The finding was corroborated by the suggestions of several researchers (e.g., Struminsky 2005; Grechnev et al. 2008; Aschwanden 2012; Kurt et al. 2013; Firoz et al. 2019). Apart from those arguments, some other researchers (e.g., Nitta et al. 2012; Grechnev et al. 2013) emphasized the magnetic field connection of the active region with the observer on the Earth or near Earth's space, thus leading to the suggestion that even a weak flare and CME can cause a GLE.

In practice, the CME stems from the same origin the flare generates from, and the strength of the spatial relation between flares and CMEs depends on the magnetic configurations involved in the solar eruption (e.g., see Low 1996; Hundhausen 1999; Aschwanden 2002, 2006; Firoz et al. 2010). Such related arguments have been illustrated by Aschwanden (2012), in line with several other researchers (e.g., Harrison 1995; Kurt et al. 2004; Jing et al. 2005; Kuznetsov et al. 2006; Chupp & Ryan 2009); for instance, the flares trigger earlier than CMEs. This was supported by some other researchers (e.g., Firoz et al. 2019) that the CME first onsets occur after flare first onsets, and the flare impulsive phase evolves with the CME acceleration phase almost simultaneously (e.g., Jang et al. 2017); thus, the CMEs alone most likely cannot produce GLEs (e.g., Firoz et al. 2011a, 2011b). The relative importance/or impact of the flares and CMEs seems to be the key factor to understanding the GLE productions (e.g., Cane et al. 2002, 2007; Firoz et al. 2015).

Those statements motivated us to carry out an investigation of the relation between flare fluences and CME speeds during some GLE-SEPs (SEPs associated with GLEs) and non-GLE-SEPs (SEPs with no GLEs). Earlier, Andriopoulou et al. (2011b) touched this issue on GLEs while explaining the characteristics of the related flares, CMEs, and radio bursts to understand their relationships with the GLEs. To our knowledge, there was no detailed exploration of the relation between the flare fluences and CME speeds so as to comprehend the GLE mechanism. We carried out the present study in detail over some GLE-SEP and major non-GLE-SEP events. This paper is arranged as follows. Observation and data analysis are described in Section 3, results and discussion are given in Section 4, some disparate non-GLEs are illustrated in Section 5, and a general discussion is given in Section 6. The summary and conclusion are noted in Section 7.

3. Observation, Data Treatment, and Analysis

3.1. Selection of the Events

Firoz et al. (2019) defined the GLE-SEPs and non-GLE-SEPs while selected 13 GLE-SEP events and 23 non-GLE-SEP events for 1997–2012. The study followed the GLE events listed in the catalog of the Neutron Monitor Data Base (NMDB; http://www.nmdb.eu/nest/; e.g., Mavromichalaki et al. 2011) and SEP events listed in the catalog of NASA (https://umbra.nascom.nasa.gov/SEP/; e.g., Reames 1999; Tylka et al. 2005). The proton flux intensity (cm^{-2} sr^{-1} s^{-1}) of $>$10 MeV and cosmic-ray flux intensity (counts s^{-1}) have been retrieved from the OMNI-NASA (https://omniweb.gsfc.nasa.gov/; e.g., King & Papitashvili 2005) and Oulu Neutron Monitor (e.g., Usoskin et al. 2001), respectively. Since the selected GLE-SEP events were associated with a $>$M5 flare, likewise, non-GLE-SEP events associated with a $\geqslant$M4.7 ($\sim$M5) flare were selected.

In the selected event list, the GLE58, GLE61, and GLE68 events were excluded, as the results for these three events were found to be ambiguous due to some observational errors. For example, over GLE58 and GLE61, the flare lay behind the limb, and the thermal X-ray-emitting arcades were mostly occulted; also, the CME contained a data gap in the spatial resolution (e.g., Grechnev et al. 2017). The GLE68 was an extremely weak event with a smaller peak increase ($\leqslant$3%) recorded by only a few neutron monitors; hence, researchers examined it by using the GLE alert signal algorithm and found GLE68 undetectable as it appeared on the elevated background (e.g., Kuwabara et al. 2006; Reames 2009; Mavromichalaki et al. 2010; Andriopoulou et al. 2011b; Souvatzoglou et al. 2014). In this study, we have exploited the selected events of Firoz et al. (2019), with one more event (GLE66; 2003 October 29) included, as it was associated with a very strong flare (X10.0; e.g., Andriopoulou et al. 2011b). Thus, this study is based on 14 GLE-SEP and 23 non-GLE-SEP events (see Tables 1 and 2).

3.2. Flare Fluence and CME Speed

Flare fluence. The flare fluences are calculated by integrating the *GOES* soft X-ray (SXR; 1–8 Å) fluxes subtracted by the mean background. The mean background is the average of the fluxes over a suitable time interval before the onset time and/or in the case after the possible end time or before the time it starts rising again at the start of a subsequent flare (e.g., Emslie et al. 2012). Determination of the total fluence (fluence over the whole phase) is indeed difficult, because there is no commonly recognized method to specify the end time of the SXR burst (e.g., Salas-Matamoros & Klein 2015). Researchers used different abstractions to define the SXR end time. For instance, Kahler et al. (1989) defined the end time as the time the SXR returns to the *GOES*/NOAA C2 level, whereas Yashiro & Gopalswamy (2009)

Table 1
Over 14 GLE-SEP Events Associated with Flares >M4.7 ($\sim$M5)

Event	Date	*GOES*/NOAA Flare								CME				χ^2		
GLE	(D.M.Y)	Class	Location	AR	$T_{\rm st}$	$T_{\rm pk}$	$T_{\rm nd}$	Flare Fluence φ		$T_{\rm apr1}$	Speed $V_{\rm cme}$	CPA	AW	Bet^n φ_w and $V_{\rm cme}$	Bet^n φ_r and $V_{\rm cme}$	Bet^n φ_d and $V_{\rm cme}$
					(UT)	(UT)	(UT)	st-pk φ_r (J m^{-2})	st-end φ_w (J m^{-2})	(UT)	(km s^{-1})	(deg)	(deg)	χ^2_w	χ^2_r	χ^2_d
55	1997 Nov 6	X9.4	S18W63	8100	11:49	11:55	13:12	0.127	0.516	12:10:41	1556	Halo	360	0.004	0.094	2.5E−6
56	1998 May 2	X1.1	S15W15	8210	13:31	13:42	17:21	0.022	0.107	14:06:12	938	Halo	360	0.605	1.708	0.505
57	1998 May 6	X2.7	S11W65	8210	7:58	8:09	9:58	0.073	0.292	08:29:13	1099	309	190	2.198	3.653	1.926
59	2000 Jul 14	X5.7	S22W07	9077	10:08	10:24	13:09	0.223	1.256	10:54:07	1674	Halo	360	1.359	0.364	1.817
60	2001 Apr 15	X14.4	S20W85	9415	13:42	13:50	15:13	0.345	1.130	16:06:31	1199	245	167	11.048	12.451	10.349
62	2001 Nov 4	X1.0	N06W18	9684	16:03	16:20	22:56	0.042	0.410	16:35:06	1810	Halo	360	2.052	5.421	1.418
63	2001 Dec 26	M7.1	N08W54	9742	04:32	05:40	11:32	0.104	0.473	05:30:05	1446	281	>212	0.176	0.274	0.178
64	2002 Aug 24	X3.1	S02W81	10069	00:49	01:12	7:38	0.188	0.843	01:27:19	1913	Halo	360	0.260	0.316	0.235
65	2003 Oct 28	X17.0	S16E08	10486	11:00	11:10	12:48	0.606	2.589	11:30:05	2459	Halo	360	0.058	0.381	0.026
66	2003 Oct 29	X10.0	S15W02	10486	20:37	20:49	01:04*	0.355	1.390	20:54:05	2029	Halo	360	1.8E−4	0.003	8.9E−4
67	2003 Nov 2	X8.3	S14W56	10486	17:03	17:25	20:45	0.410	1.492	17:30:05	2598	Halo	360	2.684	2.410	2.964
69	2005 Jan 20	X7.1	N14W61	10720	6:36	7:01	18:30	0.532	2.394	06:54:05	2800	Halo	360	1.704	2.879	1.481
70	2006 Dec 13	X3.4	S06W23	10930	2:14	2:40	8:10	0.244	0.871	02:54:04	1774	Halo	360	0.007	0.111	7.9E−4
71	2012 May 17	M5.1	N11W76	11476	1:25	1:47	5:40	0.034	0.162	01:48:05	1582	Halo	360	4.723	2.888	5.059

Note. The first and second columns contain GLE event numbers and occurrence dates. The third through tenth columns contain the flare properties such as class, location, active region (AR), possible start ($T_{\rm st}$), peak ($T_{\rm pk}$), possible end time ($T_{\rm end}$), and fluence over rise (φ_r) and whole (φ_w) phases based on *GOES* X-ray fluxes. The 11th–14th columns contain CME properties such as CME first appearance ($T_{\rm apr1}$), speed ($V_{\rm cme}$), central position angle (CPA), and angular width (AW). The 15th–17th columns contain χ^2 ($\chi^2 = [\{\log_{10}V_{\rm cme} - y{\rm fit}\}/\sigma\{\log_{10}V_{\rm cme}\}]^2$) values between (Bet^n), the observed data points, and the corresponding statistical data points on the linear fit line. An asterisk indicates the flare end time in the following day. More parameters of these events are given in Firoz et al. (2019).

Table 2
Over 23 Non-GLE-SEP Events Associated with Flares of ⩾M4.7 (∼M5)

Event (D.M.Y)	NOAA/*GOES* Flare								CME				χ^2		
	Class	Location (deg)	AR	T_{st} (UT)	T_{pk} (UT)	T_{end} (UT)	Fluence φ St-peak (J m^{-2})	Fluence φ St-End (J m^{-2})	T_{apr1} (UT)	Speed V_{cme} (km s^{-1})	CPA (deg)	AW (deg)	Bet^n φ_w and V_{cme} χ_w^2	Bet^n φ_r and V_{cme} χ_r^2	Bet^n φ_d and V_{cme} χ_d^2
1997 Nov 4	X2.1	S14W33	8100	05:52	05:58	06:02	0.02084	0.0856	06:10:05	785	Halo	360	8.73855	8.08008	9.84191
2000 Jun 10	M5.2	N22W38	9026	16:40	17:02	17:19	0.02642	0.11146	17:08:05	1108	Halo	360	1.47598	1.26047	1.81124
2000 Nov 8	M7.4	N10W77	9213	23:04	23:28	00:05	0.0597	0.2287	23:06:05	1738	271	>170	0.46909	0.38669	0.45512
2000 Nov 24	X2.3	N22W07	9236	15:05	15:13	15:21	0.07088	0.21407	15:30:05	1245	Halo	360	1.41721	2.07845	1.33135
2001 Mar 29	X1.7	N20W19	9393	09:57	10:15	10:32	0.1332	0.32633	10:26:05	942	Halo	360	10.4724	10.7374	10.8503
2001 Apr 2	X20.	N19W72	9393	21:32	21:51	22:03	0.55024	2.97777	22:06:07	2505	261	244	0.05772	0.23957	0.07934
2001 Apr 10	X2.3	S23W09	9415	05:06	05:26	05:42	0.12258	0.48476	05:30:00	2411	Halo	360	3.37433	3.11282	3.57154
2001 Oct 1	M9.1	S20W84	9628	04:41	05:15	05:23	0.04839	0.44639	05:30:05	1405	Halo	360	1.49649	0.14168	2.01603
2002 Apr 21	X1.5	S14W84	9906	00:43	1:51	02:38	0.24862	0.93197	01:27:20	2393	Halo	360	1.29556	1.03878	1.51895
2002 Nov 9	M4.7	S12W29	10180	13:08	13:23	13:36	0.02001	0.06952	13:31:45	1838	Halo	360	4.85737	4.10193	4.80918
2003 May 28	X3.6	S07W20	10365	00:17	00:27	00:39	0.09783	0.55894	00:50:05	1366	Halo	360	2.60013	1.52656	2.99183
2003 May 31	M9.3	S07W65	10365	02:13	02:24	02:40	0.02355	0.15601	02:30:19	1835	Halo	360	1.91649	3.4381	1.52159
2003 Oct 26	X1.2	N02W38	10484	17:21	18:19	19:21	0.21117	0.94962	17:54:05	1537	270	>171	2.12349	1.77085	2.19388
2003 Nov 4	X17.4	S19W83	10486	19:38	19:57	20:06	0.28956	1.74747	19:54:05	2657	Halo	360	1.24832	2.1362	1.26537
2004 Nov 7	X2.0	N09W17	10696	15:56	16:06	16:15	0.11878	0.40523	16:54:05	1759	Halo	360	0.03294	4.215E−5	0.05614
2005 Jul 14	X1.2	N11W90	10786	10:16	10:55	11:29	0.18424	0.58493	10:54:05	2115	Halo	360	0.78556	0.37971	1.02332
2005 Aug 22	M5.6	S13W65	10798	16:46	17:27	18:02	0.08236	0.24145	17:30:05	2378	Halo	360	6.0282	4.33146	6.76883
2011 Aug 4	M9.3	N19W36	11261	03:49	03:57	04:04	0.02569	0.10323	04:12:05	1315	Halo	360	0.0199	0.01512	0.0556
2011 Aug 9	X6.9	N17W69	11263	07:59	08:05	8:08	0.11871	0.25572	08:12:06	1610	Halo	360	0.01631	0.24519	0.17738
2012 Jan 23	M8.7	N28W21	11402	3:38	3:59	4:34	0.053	0.22442	04:00:05	2175	Halo	360	4.0369	4.05154	3.99119
2012 Jan 27	X1.7	N27W71	11402	18:03	18:37	18:56	0.15154	0.4337	18:27:52	2508	Halo	360	4.74389	3.15924	5.59758
2012 Mar 13	M7.9	N17W66	11429	17:12	17:41	18:25	0.07455	0.3347	17:36:05	1884	Halo	360	0.59702	0.73762	0.54625
2012 Jul 12	X1.4	S15W01	11520	16:16	16:49	17:30	0.1874	0.58526	16:48:05	885	Halo	360	17.5129	18.8734	17.6973

Note. The second through ninth columns contain the flare properties, such as class, location, active region (AR), possible start (T_{st}), peak (T_{pk}), possible end time (T_{end}), and fluence over rise (φ_r) and whole (φ_w) phases based on NOAA/*GOES* X-ray fluxes. The 10th–13th columns contain CME properties such as CME first appearance (T_{apr1}), speed (V_{cme}), central position angle (CPA), and angular width (AW). The 14th–16th columns contain χ^2 ($\chi^2 = [\{\log_{10} V_{cme} - y\mathrm{fit}\}/\sigma\{\log_{10} V_{cme}\}]^2$) values between (Bet^n) and the observed data points and corresponding statistical data points on the linear fit line. More parameters of these events are given in Firoz et al. (2019).

considered the end time when the SXR flux decays to half of the peak value. In this study, we considered the end time of a flare to be at the point where the SXR decay phase ends to the same or similar intensity of start time after the background subtraction (e.g., Firoz et al. 2014b; Grechnev et al. 2015a; Grechnev & Kochanov 2016). The observational data of SXR (1–8 Å) fluxes were retrieved from NOAA/*GOES* (https://www.ngdc.noaa.gov/stp/satellite/goes/dataaccess.html; e.g., Krucker & Benz 1998). Note that the flare end times we utilized for the determination of flare fluences sometimes vary from those given in the NOAA/*GOES* catalog (e.g., Aschwanden & Freeland 2012; Li et al. 2016). The fluences over the whole phase (ϕ_w), rise phase (ϕ_r) and decay phase (ϕ_d) of the flare have been computed as follows (e.g., Veronig et al. 2002),

$$\phi_w = \int_{t_0}^{t_0+T_w} f_{\rm sxr}(t)dt,$$

$$\phi_r = \int_{t_0}^{t_0+T_r} f_{\rm sxr}(t)dt,$$

$$\phi_d = \int_{t_p}^{t_p+T_d} f_{\rm sxr}(t)dt,$$

where $f_{\rm sxr}(t)$ represents the temporal evolution of SXR (1–8 Å) fluxes; ϕ_w, ϕ_r, ϕ_d represent the flare fluence over the flare whole, rise, and decay phases; T_w, T_r, T_d represent the flare whole, rise, and decay duration; and t_0, t_p represent the onset and peak time, respectively.

CME kinematics. Depending on the data availability, we checked the CME kinematics using the observational remote-sensing data of the Large Angle and Spectrometric Coronagraph (LASCO) and EUV Imaging Telescope (EIT; e.g., Brueckner et al. 1995). LASCO, on board the *Solar and Heliospheric Observatory* (*SOHO*), covers the corona from 1.1 to 30 $R_\odot$, while the EIT, also on board *SOHO*, observes the Sun's disk and corona up to 1.5 $R_\odot$ (e.g., Delaboudiniere et al. 1995; Cyr et al. 2000). The LASCO instrument consists of a set of three nested coronagraphs (C1: 1.1–3 $R_\odot$; C2: 2–6 $R_\odot$; C3: 4–30 $R_\odot$) with overlapping and concentric fields of view (FoVs; e.g., Schwenn et al. 1997). We used the measurements of C2 (FoV 2–6 $R_\odot$) and C3 (FoV 4–30 $R_\odot$) of the LASCO, because they observe the CME evolution in the middle and high coronae. More details can be studied in some papers (e.g., Domingo et al. 1995; Zhang et al. 2001; Simnett 2006).

Further, we analyzed the white-light evolution in the corona observed by the COR2 coronagraphs (FoV 2.5–15.0 $R_\odot$) of the Sun–Earth Connection Coronal and Heliospheric Investigation (SECCHI) on board the twin *Solar TErrestrial RElations Observatory* spacecraft (*STEREO*; e.g., Howard et al. 2008) available from 2006. The kinematics of CMEs determined from the observations by *STEREO-A* (*STA*) have been utilized, as the *STA* exposed the white-light evolution better than *STEREO-B* (*STB*). We analyzed the FITS data of the LASCO, EIT, and *STA* and compared the results with those determined by using the STEREO CME Analysis Tool (StereoCAT) provided by the NASA Community Coordinated Modeling Center (CCMC; Thernisien et al. 2009; Liu et al. 2010).

The mean of the CME speeds derived by analyzing the FITS data and determined by using StereoCAT over the same time window has been employed in order to understand the CME kinematics (e.g., Figure 1). The CME speeds were determined by using the running difference of the FITS data of the images following the process shown in Firoz et al. (2014b).

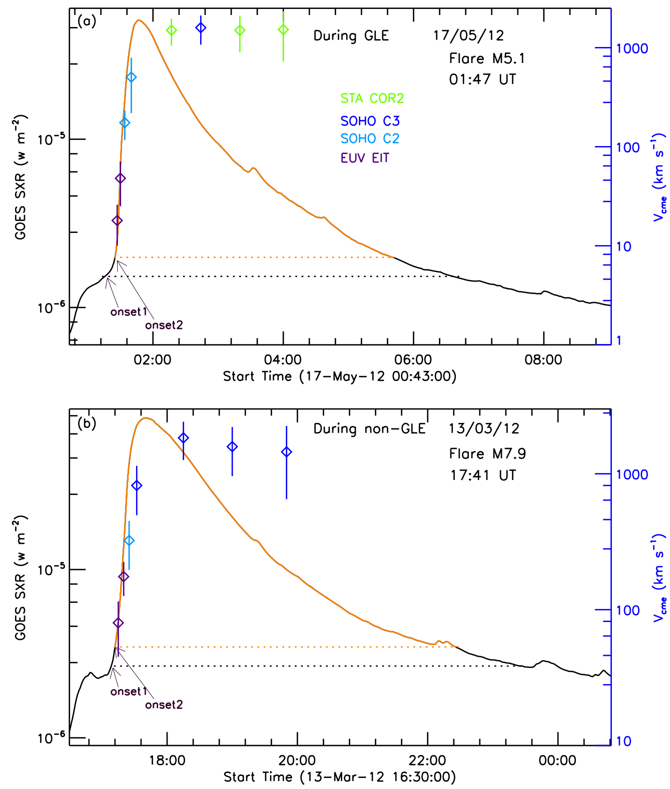

Figure 1. Temporal profiles of *GOES* X-ray (1–8 Å; SXR W m^{-2}) and measured CME speed ($V_{\rm cme}$ km s^{-1}) during a GLE-SEP event (a) and a non-GLE-SEP event (b). The dotted lines intersect the onset and end time of the flares. Parallel dotted lines determine the possible onset1 and onset2 (e.g., Zhang et al. 2001; Zhang & Dere 2006).

3.3. Significance Test for the Correlation between Flare Fluence and CME Speed

We estimated the probability (p-value) test that defines the statistical significance through the assumption of null hypothesis or/and of obtaining a result equal to or more extreme than what was actually observed. If the *p*-value is very close to the cutoff (0.05), it is considered marginal. The test rejects the null hypothesis at the prescribed significance level ($p = 0.05$). The correlation coefficient (r) is considered significant if the *p*-value of the relationship is <0.05 (e.g., Moore 2006; Firoz et al. 2010). For better comprehension, the χ^2 values have also been checked following the process (e.g., Cochran 1952; Ryabko et al. 2004). The χ^2 defines the distance between the observed data point and corresponding statistical data point.

Note that the correlation magnitude would vary if we used $V_{\rm cme} \sim 882$ (km s^{-1}) for GLE69. The $V_{\rm cme}$ ($\sim$882 km s^{-1}) was measured using the routine technique by the *SOHO*/LASCO catalog group, while Gopalswamy et al. (2005) and Simnett (2006) measured the $V_{\rm cme}$ ($\sim$2500–3242 km s^{-1}) using different measurements, thus causing an uncertainty. We investigated and measured the $V_{\rm cme} \sim 2800$ (km s^{-1}) that could possibly be compromised between Gopalswamy et al. (2005) and Simnett (2006), as illustrated by Grechnev et al. (2008). The $V_{\rm cme} \sim 2800$ (km s^{-1}) is exploited for the GLE69 event.

4. Results and Discussion

4.1. Evolution of the Flare and CME Kinematics

Figure 1 shows schematic plots of the CME kinematic evolution and its relation with the temporal evolution of the

GOES X-ray (1–8 Å; SXRL W m^{-2}) during a GLE-SEP (2012 May 17) and non-GLE-SEP (2012 March 13) event. Dotted horizontal lines intersect the start and end time of the flares. The parallel dotted lines determine the flare possible initial onset (onset1) and prompt onset (onset2) following the process illustrated by Zhang et al. (2001) and Zhang & Dere (2006). Thus, the flare onset1 and onset2 were previously determined by and listed in Firoz et al. (2019). Flare onset2 is consistent with the flare onset time given in the NOAA/*GOES* catalog (e.g., Aschwanden & Freeland 2012). So, the durations of the flares are to be determined in terms of the time difference between flare onset2 and the flare end time.

Most of the GLE-SEP-associated flares have shorter rise and longer decay phases than most of the non-GLE-SEP-associated flares, resulting in a relatively longer duration of the GLE flares, on average (e.g., Andriopoulou et al. 2011b), than the non-GLE flares (see Tables 1 and 2). However, some GLE flares have shorter durations than non-GLE flares (e.g., see Figure 1). Figure 1(a) shows a GLE-SEP-associated M5.1 class flare containing a shorter rise phase (~22 minutes) and decay phase (~3.9 hr). Figure 1(b) shows an M7.9 class flare containing a relatively longer rise phase (~29 minutes) and decay phase (~4.7 hr). The CME evolution generally undergoes three distinct phases (initiation, acceleration, and propagation), which correspond to the initial/primary phase (onset2 – onset1), rise phase, and decay phase of the associated flare, respectively (e.g., Zhang & Dere 2006; Jang et al. 2017).

Figure 1 explains that the rise phases of the SXR (1–8 Å; W m^{-2}) and CME speed (V_{cme} km s^{-1}) have similar temporal evolution, indicating that the main CME acceleration and flare rise (energy-release) phase occur almost simultaneously. Hence, the flare rise phase is more important. This is consistent with the suggestions by several researchers (e.g., Hundhausen 1993; Dryer 1994; Zhang et al. 2004; Li & Zank 2005; Grechnev et al. 2015b) that the CME acceleration and flare rise phases are intimately related, as the flare and CME originate from the same magnetic reconnection. Figure 1(a) demonstrates that the V_{cme} tends to be constant after the flare peak, while Figure 1(b) demonstrates that the V_{cme} tends to decay after the flare peak. Both cases are consistent with the findings of previous studies (e.g., Zhang et al. 2001; Cliver et al. 2005; Maričić et al. 2007; Salas-Matamoros & Klein 2015) that CME propagates at nearly constant speed or decreases after the flare peak, thus indicating a correlation between the terminal speed of CME and the SXR flare.

4.2. Association between Flare Fluence and CME Speed

Figures 2 and 3 contain the distributions of the data points of observed flare fluence (ϕ) and CME speed (V_{cme}) over the flare whole, rise, and decay phases of the GLEs and non-GLEs. Figure 2 shows that the mean ϕ_w (~0.994 J m^{-2}) over the flare whole phase of the GLEs is almost two times that (~0.542 J m^{-2}) of the non-GLEs, whereas their mean V_{cme} (1776–1756 km s^{-1}) differs slightly, indicating that the flares dominate the GLE productions.

Further, Figure 3 shows that the mean ϕ_r (~0.236 J m^{-2}) over the flare rise phases of the GLEs is almost two times the ϕ_r (~0.128 J m^{-2}) of the non-GLEs; similarly, the mean ϕ_d (~0.758 J m^{-2}) over the flare decay phases of the GLEs is almost two times the ϕ_d (~0.417 J m^{-2}) of the non-GLEs. In general, these results support the previous suggestions by many researchers that the intensive flares and high-speed CMEs are

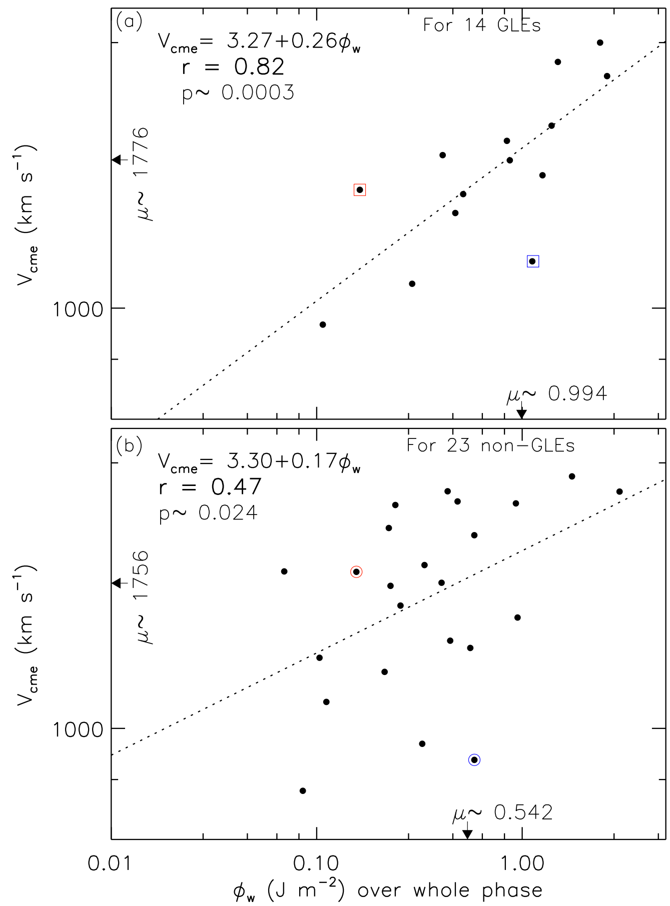

Figure 2. Logarithmic plots of CME speeds and flare fluences over the flare whole phase during 14 GLE-SEP and 23 non-GLE-SEP events (see Tables 1 and 2). The panels show the CME speed (V_{cme} km s^{-1}) vs. *GOES* X-ray (1–8 Å) fluence over the flare whole phase (ϕ_w J m^{-2}). The μ, r, and p denote the mean, correlation coefficient, and probability (p-value), respectively. The equations noted in the upper left corner of the figure follow the usual linear regression equation. (a) Two data points of GLEs that maintained a larger distance from the linear fit line are marked by red and blue squares, and (b) two similar data points of non-GLEs are marked by red and blue circles. The χ^2 values defining the distance between the observed and statistical data points are noted in Tables 1 and 2.

associated with the GLEs (e.g., Cliver 2006; Grechnev et al. 2008, 2013; Firoz et al. 2010, 2012; Aschwanden 2012). However, our main effort is to comprehend the flare–CME conjugation by analyzing the correlation strength and proportional trends between flare fluences and CME speeds.

4.3. Correlation between Flare Fluence and CME Speed

Figures 2 and 3 demonstrate the relation between flare fluence (ϕ) and CME speed (V_{cme}) in terms of the correlation coefficient (r) evaluated by the p-value. The correlation strength is clarified with the intercept value and slope of the fit line following the linear regression equation ($y = l + mx$; where x and y represent ϕ and V_{cme}, l is the intercept, and m is the slope of the fit line). The χ^2 values between the observed data points (ϕ; V_{cme}) and the corresponding statistical data points on the linear fit line are noted in Tables 1 and 2 for better understanding of the changeovers of the data points causing variations in correlation magnitude.

It is found (Figure 2) that the V_{cme} (km s^{-1}) maintains a much stronger correlation ($r = 0.82$; $p \sim 0.0003$) with the ϕ_w

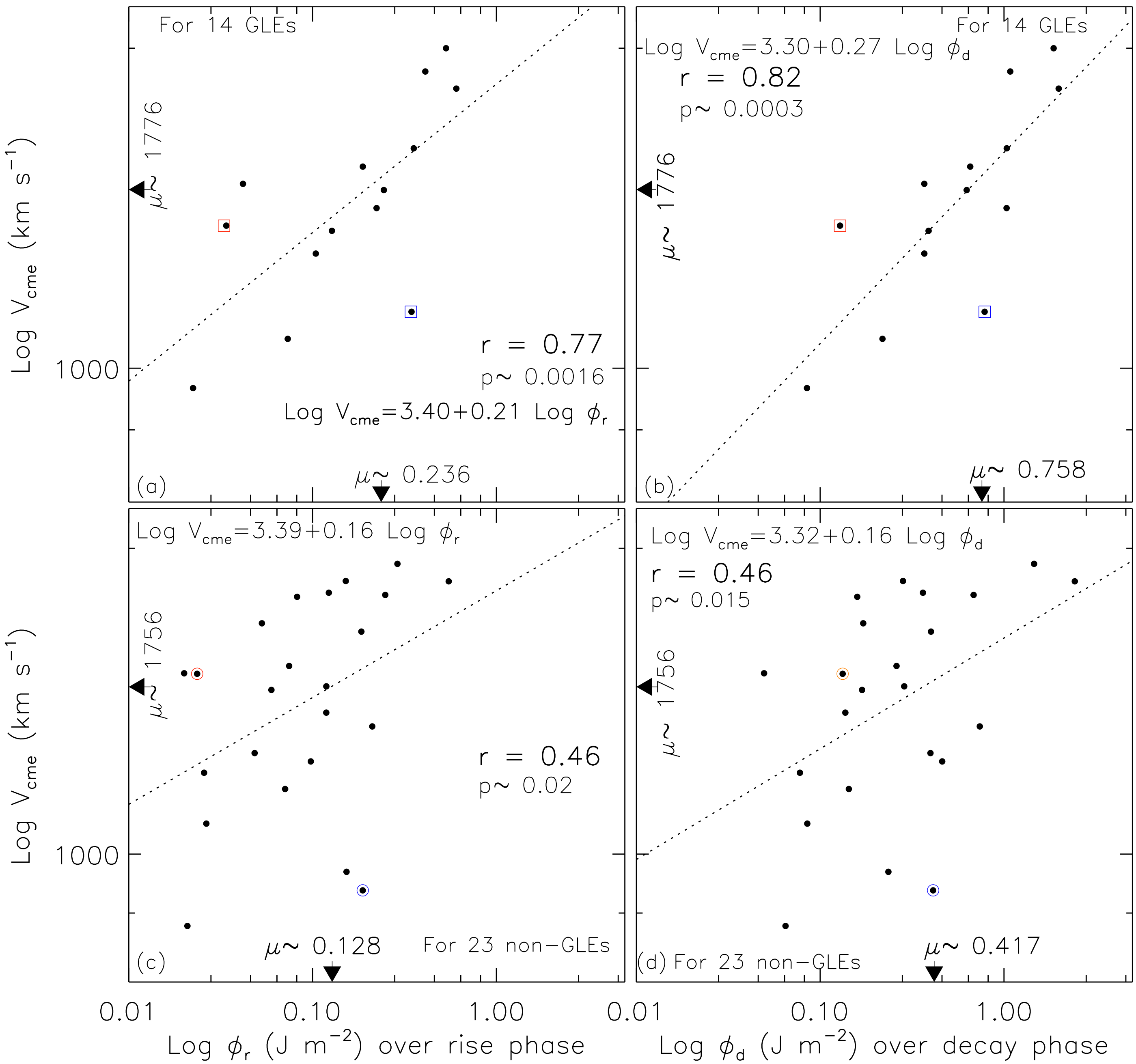

Figure 3. Logarithmic plots of CME speed (V_{cme} km s^{-1}) vs. *GOES* X-ray (1–8 Å) fluence over the flare rise (ϕ_r J m^{-2}) and decay (ϕ_d J m^{-2}) phases for 14 GLE-SEP and 23 non-GLE-SEP events (see Tables 1 and 2). The μ, r, and p denote the mean, correlation coefficient, and probability (p-value), respectively. The equations shown in the figure represent the linear regression. Two data points marked in Figure 2 are also marked here to realize their transitions over the flare rise and decay phases. The χ^2 values that define the distance between the observed and statistical data points are noted in Tables 1 and 2.

(J m^{-2}) of the 14 GLEs than that ($r = 0.47$; $p \sim 0.024$) of the 23 non-GLEs. Data points marked by red and blue squares represent the ϕ_w (J m^{-2}) and V_{cme} (km s^{-1}) associated with a disparate GLE event (GLE71, 2012 May 17; e.g., Papaioannou et al. 2014) and an exceptional GLE event (GLE60, 2001 April 15; e.g., Muraki et al. 2008), respectively. Most of the data points (ϕ_w versus V_{cme}) of the GLEs follow a near-linear trend, particularly one data point, marked by a blue square, that lessened the correlation magnitude. Another data point, marked by a red square, follows the near-linear trend weakly and impacts slightly on the correlation magnitude. (These two GLEs are to be discussed with two non-GLEs having nearly similar trends.)

Excluding the data point of GLE71, marked by the red square, gives rise to the correlation ($r = 0.86$; $p \sim 0.0002$) for 13 GLEs. Excluding the data point of GLE60, marked by a blue square, gives further rise to the correlation ($r = 0.88$; $p \sim 0.0002$) for 12 GLEs whose data points (ϕ; V_{cme}) follow a near-linear trend verified by the χ^2 values. Accordingly, some data points of non-GLEs, having χ^2 values similar to those of some GLEs, might give rise to correlation magnitudes like those of GLEs. This will be discussed later (Sections 5 and 6) in this paper.

The correlation magnitude did not vary over the flare rise and decay phases for non-GLEs, whereas it varied significantly over the flare rise phase for GLEs (see Figure 3). Three data points, including the ones associated with GLE71 and GLE60 and marked by red and blue squares over the rise phase, shifted away from the linear fit line, causing weaker correlation ($r = 0.77$) than that ($r = 0.82$) over the decay phase. Thus, the correlation magnitudes vary differently depending on the proportional trend between CME speeds and flare fluences over the whole, rise, and decay phases. The strong correlation of the data points refers to their rational proportionality, which seems to depend on the flare–CME conjugation in the magnetic reconnection. This seems to be in line with Andriopoulou et al. (2011a, 2011b), who suggested that the GLE-associated flares and CMEs might be the manifestations of the same eruptive process.

4.4. Proportional Trend between Flare Fluence and CME Speed

As observed (Figure 2(a) and Table 1), except for the data point of GLE60, marked by a blue square, the 13 data points of the GLEs follow a more or less near-linear trend, such that the $V_{\rm cme}$ increases with the increase of ϕ_w. For instance, the strongest ϕ_w ($\sim$2.589; 2.3942 J m^{-2}) is associated with the highest $V_{\rm cme}$ ($\sim$2459; 2800 km s^{-1}), while the weakest ϕ_w ($\sim$0.1071 J m^{-2}) is associated with the lowest $V_{\rm cme}$ (938 km s^{-1}). Thus, most of the data points of the GLEs maintain more or less rational proportionality leading to the near-linear trend. However, exceptions may be observed. For example, the ϕ_w ($\sim$1.1298 J m^{-2}) of GLE60 shows a very weak proportion with its associated $V_{\rm cme}$ (1199 km s^{-1}), with the flare being much more dominant. The data point ($\sim$0.16213 J m^{-2}; 1582 km s^{-1}) of GLE71 resulting in a weak proportion follows the near-linear trend weakly (e.g., Firoz et al. 2015).

It is found (Figure 2(b) and Table 2) that the data point ($\sim$0.15601 J m^{-2}; 1835 km s^{-1}) of the non-GLE of 2003 May 31, marked by a red circle, seems to have a proportional trend similar to that of GLE71, while the data point ($\sim$0.58526 J m^{-2}; 885 km s^{-1}) of the non-GLE of 2012 July 12, marked by a blue circle, seems to maintain a nearly similar trend to that of the exceptional GLE60. The GLE60 and GLE71 are to be compared with the two non-GLEs (2012 July 12; 2003 May 31).

4.5. Comparison between the GLE on 2001 April 15 and Non-GLE on 2012 July 12

4.5.1. GLE on 2001 April 15

The GLE on 2001 April 15 (GLE60) is an exceptional GLE event originating from the southwestern hemisphere (S20° W85°). The event took place with a very strong flare (X14.4) and relatively slow $V_{\rm cme}$ ($\sim$1199 km s^{-1}), showing an unusual proportion between the ϕ_w ($\sim$1.1298 J m^{-2}) and $V_{\rm cme}$ ($\sim$1199 km s^{-1}) compared to those of most of the GLEs. This is the only GLE that corresponds to the longest time delay ($\sim$136 minutes) between the flare peak and CME first appearance (see Table 1). In this event, Tylka et al. (2002) found that both flare and CME acceleration mechanisms are operating, with the flare being more powerful. In practice, as revealed by Muraki et al. (2008), this flare developed atypically with three-step acceleration and different dynamical behaviors of the magnetic loops operating in each step of the acceleration, thus resulting in relatively more fluence over the rise phase (see Table 1). It is found (Figures 2(a) and 3(a)–(b)) that the correlation magnitude decreased over the whole phase of the flare due to this event being shifted ($\chi^2 = 12.45$) away from the linear fit line, while it increased significantly over the decay phase of the flare due to being shifted ($\chi^2 = 10.35$) toward the linear fit line. However, over the rise phase of the flare, this event shifted moderately ($\chi^2 = 11.05$), although the correlation magnitude decreased due to some other data points shifting conspicuously compared to those over the whole and decay phases (see χ^2 values in Table 1). Thus, it is observed that the $V_{\rm cme}$ ($\sim$1199 km s^{-1}) finally maintains a rational proportionality with the ϕ_d ($\sim$0.784 J m^{-2}) over the flare decay phase. Thus, GLE60 can be compared with a nearly similar data point of a non-GLE.

4.5.2. Non-GLE on 2012 July 12

It is observed that the trend of the data point (ϕ; $V_{\rm cme}$) of GLE60, marked by a blue square, is similar to that of a non-GLE (2012 July 12), marked by a blue circle (Figure 2). The data point of this non-GLE consists of a relatively low $V_{\rm cme}$ ($\sim$885 km s^{-1}) and strong ϕ_w ($\sim$0.5853 J m^{-2}). Though the proportional trend of the data point of this non-GLE is apparently similar, it is indeed different from that of GLE60 (e.g., Zucca et al. 2017). For example, the positions ($\chi^2 = 17.51$; 18.87; 17.70) of the non-GLE over the whole, rise, and decay phases of the flare are much more alienated from the linear fit line than those ($\chi^2 = 12.45$; 11.05; 10.35) of GLE60, exposing a big difference in the proportional trend (see Figures 2 and 3; Tables 1 and 2). In fact, the flare of this non-GLE originated from the location (S15° W01°) that was very close to the solar disk center. Note that the location close to the solar disk center is not an ideal position for the flare to cause GLE, because high-energy particles originating from the flare close to/at disk center mostly miss the Earth, as the Sun's magnetic fields turn spiral due to the Sun's rotation (e.g., Hu et al. 2016; Wang et al. 2016). Although the flare of GLE60 (2001 April 15) also originated from the southwestern hemisphere (S20° W85°), the location was away from the solar disk center.

4.6. Comparison between the GLE on 2012 May 17 and non-GLE on 2003 May 31

4.6.1. GLE on 2012 May 17

The GLE on 2012 May 17 (GLE71) is the only front-side GLE event of solar cycle 24 (e.g., Battarbee et al. 2018). It consists of a higher $V_{\rm cme}$ ($\sim$1582 km s^{-1}) with a relatively weak flare (M5.1) originating from the northwestern hemisphere (N11° W76°). For this disparate GLE event, Gopalswamy et al. (2013) stated that the CME was preceded by a hot ejecta (>6 MK) about 40 minutes earlier from the same active region with a speed of $\sim$70 km s^{-1}, which was overtaken by the main CME. In fact, as demonstrated by Shen et al. (2013), this event was associated with compound twin CMEs taking place within a little time difference such that the material inside the first CME's driver had been processed by the second CME, resulting in a relatively higher CME speed. This was supposed to have played an important role in conjunction with the flare impulsive phase in accelerating the GLE71 particle, though the seed particle was initiated primarily by the flare initial phase (e.g., Firoz et al. 2014a, 2014b, 2015, 2019). The data point (ϕ; $V_{\rm cme}$) of this event is marked by a red square (see Figures 2 and 3). It is found that the data point ($\phi_w \sim 0.16213$ J m^{-2}; $V_{\rm cme} \sim 1582$ km s^{-1}) over the flare whole phase lies closer ($\chi^2 = 4.72$) to the linear fit line, while the data point ($\phi_d \sim 0.1282$ J m^{-2}; $V_{\rm cme} \sim 1582$ km s^{-1}) over the flare decay phase shifted away ($\chi^2 = 5.06$) from the linear fit line, thus maintaining a weak proportionality between the flare fluence and CME speed. However, the data point ($\phi_r \sim 0.0339$ J m^{-2}; $V_{\rm cme} \sim 1582$ km s^{-1}) over the flare rise phase shifted greatly ($\chi^2 = 2.89$) toward the linear fit line, maintaining a better proportionality. The proportional trend of the data point (ϕ; $V_{\rm cme}$) of GLE71 is to be compared with a similar proportional trend of that of a non-GLE.

4.6.2. Non-GLE Event on 2003 May 31

The GLE71 (2012 May 17) originated from the northwestern hemisphere (N11° W76°), whereas the 2003 May 31 non-GLE originated from the southwestern hemisphere (S07° W65°). The common feature of these two events shows that they both originated from the location away from the solar disk center. This non-GLE was associated with an intense M-class (M9.3) flare and fast CME ($\sim$1835 km s^{-1}). The proportional trend of the data point (ϕ; $V_{\rm cme}$) of this non-GLE, marked by a red circle, is similar to that of GLE71, marked by a red square (see Figures 2 and 3; Tables 1 and 2). Thus, there is an indication that this non-GLE should have appeared as a GLE event! For instance, the data point ($\phi_w \sim 0.156$ J m^{-2}; $V_{\rm cme} \sim 1835$ km s^{-1}) over the flare whole phase lies close ($\chi^2 = 1.92$) to the linear fit line, while the data point ($\phi_w \sim 0.156$ J m^{-2}; $V_{\rm cme} \sim 1835$ km s^{-1}) over the decay phase shifted closer ($\chi^2 = 1.52$) to the linear fit line, thus maintaining a better proportionality between ϕ (J m^{-2}) and $V_{\rm cme}$ (km s^{-1}). The data point of GLE71 over the flare whole phase lies relatively away ($\chi^2 = 4.72$) from the linear fit line and ($\chi^2 = 5.01$) over the decay phase (see Table 1). The data point of GLE71 is positioned ($\chi^2 = 2.88$) close to the linear fit line over the flare rise phase, while the data point of the non-GLE is positioned ($\chi^2 = 1.52$) even closer to the linear fit line over the decay phase, which is usually associated with the CME propagation phase. On this non-GLE event, some researchers (e.g., Hanuise et al. 2006; Dayeh et al. 2010; Haider et al. 2012) demonstrated that the flare active region developed rapidly into a complex and dynamic magnetic field region with more than 70 visible sunspots. It became the dominant flare-productive region on the visible solar disk and produced a series of four flares. The fourth flare (M9.3) and $V_{\rm cme}$ ($\sim$1835 km s^{-1}) associated with this event originated from the same active region. This event underwent a geomagnetic storm, which was associated with an annular solar eclipse. This might be why this non-GLE-SEP experienced a small peak ($\sim$27 cm^{-2} sr^{-1} s^{-1}). Also note that the onset of this non-GLE-SEP emerged after the flare prompt onset, whereas the GLE-SEP onset usually emerges before the flare prompt onset (see Firoz et al. 2019).

4.7. Correlation between Flare Peak Fluence and CME Speed

Figures 4(a) and (b) show that the flare peak fluences and CME speeds are weakly correlated ($r = 0.46$; 0.41) for both GLEs and non-GLEs. This is similar to the values reported previously by several researchers (e.g., Moon et al. 2002; Vršnak et al. 2005; Yashiro & Gopalswamy 2009; Bein et al. 2012). The correlation strength between the flare peak and CME speed is more often weak, likely because the CME main acceleration pronounces over the flare rise phase and ceases over/around the flare peak (see Figure 1; see also, e.g., Qiu et al. 2004; Zhang et al. 2004; Li & Zank 2005).

The mean peak flare fluence $\phi_{\rm pk}$ ($\sim$0.038 J m^{-2}) of GLEs is about two times that ($\sim$0.019 J m^{-2}) of the non-GLEs. Investigation into the flares of GLEs for a longer period (1990–2012) exposed a very similar mean flare peak $\phi_{\rm pk}$ ($\sim$0.0378 J m^{-2}). Though the ϕ_w over the whole phase for some events with a short time duration is dominated by the flare peak $\phi_{\rm pk}$, the flare peak flux does not blur the correlation between the flare rise phase and CME speed (e.g., Maričić et al. 2007; Salas-Matamoros & Klein 2015). This is evident in Figures 4(c)–(d), which shows that after exclusion of the flare peak $\phi_{\rm pk}$, the correlation coefficient $r = 0.82$ ($p \sim 0.0003$) between the ϕ_{rp} over ascending phase and $V_{\rm cme}$ of the GLE events also appears much better than the correlation coefficient $r = 0.43$ ($p \sim 0.03$) of the non-GLEs. This indicates that the flare peak fluence or strength does not control the occurrence of GLEs; rather, the fluence over the whole and/or rise phase does. Thus, the dependence of the GLE occurrence seemingly lies on the proportional trend between flare fluence and CME speed, not the flare peak or strength.

5. Some Disparate Non-GLE-SEPs

As illustrated earlier in Section 4.3, the data points (ϕ_w J m^{-2} versus $V_{\rm cme}$ km s^{-1}) of GLE-SEP events maintain a strong correlation, while those of non-GLE-SEP events maintain a weak correlation. However, some data points (ϕ_w J m^{-2} versus $V_{\rm cme}$ km s^{-1}) of non-GLE-SEP events apparently follow proportional trends similar to some of those of the GLE-SEP events, as also realized by means of χ^2 values (see Figure 2; Tables 1 and 2). Ten such data points of ϕ_w (J m^{-2}) versus $V_{\rm cme}$ (km s^{-1}) have been selected from Figure 2 and reanalyzed in Figure 5. The selection criteria include the following: (i) the χ^2 values of the data points of GLEs should be similar to those of non-GLEs, and (ii) the m type II burst must be available to realize whether the coronal shock and flare onsets emerged before or after the SEP injection onsets at the Sun (e.g., Firoz et al. 2019).

In Figure 5, the range of χ^2 values (0.01–2.68) of the data points of 10 GLEs are nearly similar to the range of χ^2 values (0.02–2.60) of the data points of 10 non-GLEs. Note that the data points of the 10 non-GLEs still maintain a relatively weak correlation ($r = 0.72$; $p \sim 0.018$), whereas the data points of the 10 GLEs maintain a strong correlation ($r = 0.89$; $p \sim 0.0006$). Four data points marked by green circles (Figure 5(b)) have no correlation. The four data points belong to the SEP events that had onsets before both m type II and flare prompt onsets nearly at the Sun, like the GLE-associated SEPs (e.g., Firoz et al. 2019). Therefore, these four non-GLE-SEPs can be deemed atypical non-GLE-SEP events. These atypical non-GLEs-SEP events took place on 2000 November 8 and 24, 2003 October 26, and 2011 August 9 (see Table 2).

It is observed (Figure 6) that onsets of the GLE-associated SEPs emerged more or less before the flare prompt and m type II onsets, whereas most of the non-GLE-SEP onsets often emerged well after the flare prompt and type II onsets. However, the four non-GLE-SEP onsets emerged before the flare prompt and type II onsets, like those of the GLE-SEPs (Figures 6(a)–(b)). Earlier, Firoz et al. (2019) reported that the SEPs having onsets earlier than the m type II onsets most likely initiated over the flare initial (primary) phase, while the SEPs having onsets later than the m type II onsets seem to be initiated over the coronal shocks associated with flare

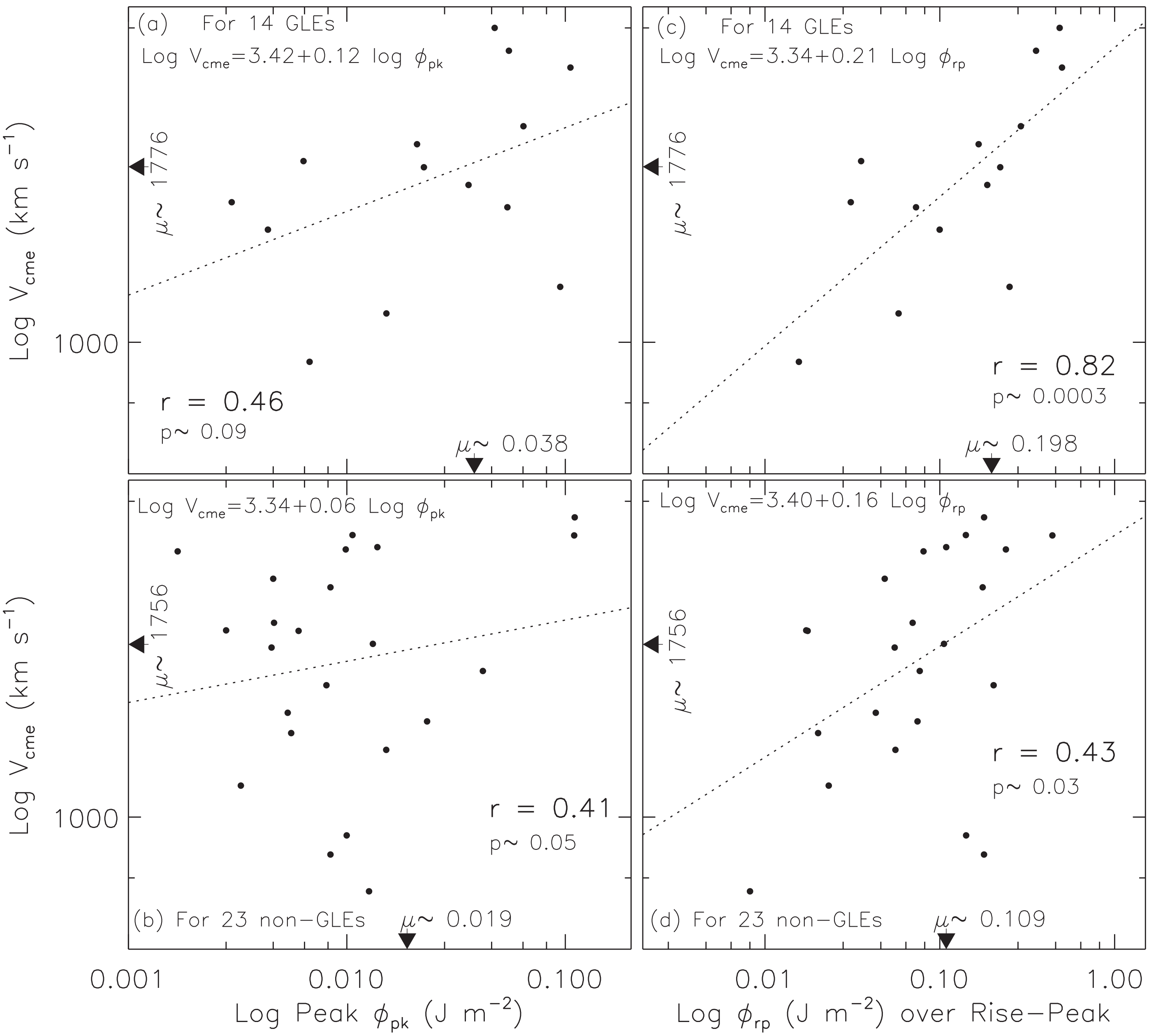

Figure 4. Logarithmic plots of CME speeds vs. fluences of the flare peak and rise phase excluding the peak during 14 GLE-SEP and 23 non-GLE-SEP events. (a) and (b) CME speed (V_{cme}; km s^{-1}) vs. *GOES* X-ray (1–8 Å) peak fluence (ϕ_{pk}; J m^{-2}) for GLEs and non-GLEs. (c) and (d) V_{cme} (km s^{-1}) vs. fluence of rise phase excluding peak fluence ϕ_{rp} (J m^{-2}) for GLEs and non-GLEs. The mean values (μ) for V_{cme} (km s^{-1}), ϕ_{pk} (J m^{-2}), and ϕ_{rp} (J m^{-2}) are indicated by arrows.

impulsive phases or flare drivers (e.g., Klassen et al. 1999, 2002).

5.1. Review of the Four Atypical Non-GLE-SEP Events

Non-GLE-SEP event on 2000 November 8. Lots of studies related to this event were carried out (e.g., Cane et al. 2003; Nitta et al. 2003; Ruffolo et al. 2003; Grechnev et al. 2015b, 2017; Thakur et al. 2016). Their illustrations indicate that this event was exceptional. For instance, Nitta et al. (2003) observed that this event appears to have originated in the nonactive region eruption rather than the M7.4 flare. This otherwise supported Cane et al. (2003), who found that the event was affected by the occurrence of an immediate solar event on 2000 November 9.

Non-GLE-SEP event on 2000 November 24. The non-GLE-SEP event on 2000 November 24 was a more complex event. Three *GOES* X-class flares, X2.0, X2.3, and X1.8, occurred at about 04:55, 14:51, and 21:43 UT, respectively, from almost the same location (N19W06) within the same active region (NOAA 9236). Hence, Takasaki et al. (2004) introduced the event as a homologous flare event. Chandra & Uddin (2006) studied the first (X2.0) of the three flares, which was impulsive in nature in almost all wavelengths and was associated with a fast halo CME; also, the flare was a large eruptive or long-duration event. Pohjolainen et al. (2015) found that two propagating shocks started on 2000 November 24 and arrived near Earth on 2000 November 26.

Non-GLE-SEP event on 2003 October 26. The 2003 October 26 event is one of the large "Halloween 2003" events (e.g.,

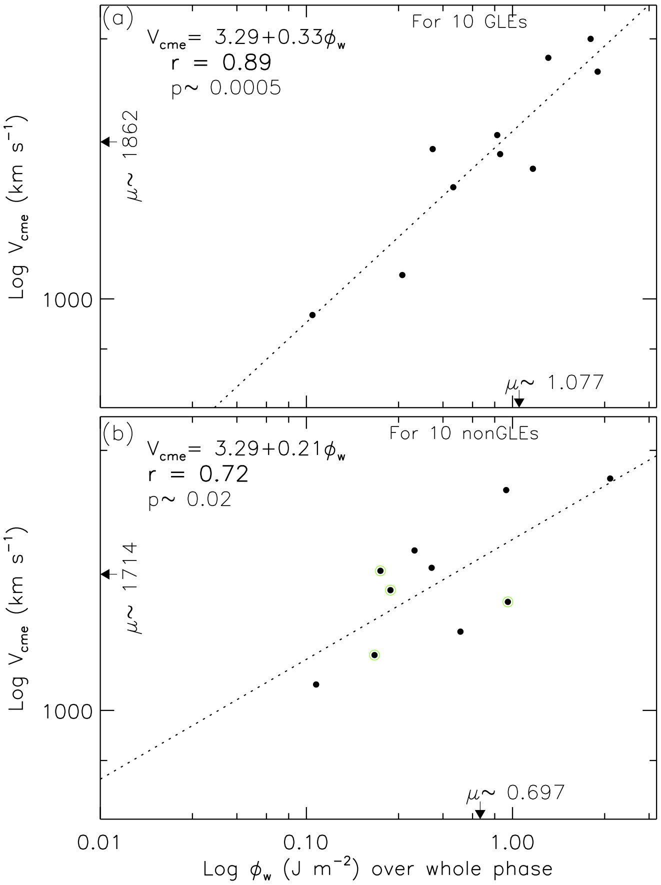

Figure 5. Logarithmic plots of CME speed ($V_{\rm cme}$ km s^{-1}) vs. *GOES* X-ray (1–8 Å) fluence over the flare whole phase (ϕ_w J m^{-2}) during (a) 10 GLE-SEP and (b) 10 non-GLE-SEP events. These data points have been selected from Figure 2. The μ, r, and p denote the mean, correlation coefficient, and probability (p-value), respectively. The equations noted in the upper left corner of the panels follow the usual linear regression equation. Four data points marked by green circles belong to the SEP events that had onsets before both the m type II burst and flare prompt onsets nearly at the Sun (see Figure 6).

Núñez 2011). Ning et al. (2005, 2008) observed that this event exposed two parts of radio bursts, presenting a contribution of both flare and CME, which seemingly maintained a good proportionality (e.g., Figure 5), indicating the possibility of GLE.

Non-GLE-SEP event on 2011 August 9. A similar plight for the non-GLE-SEP event on 2011 August 9 has been noted. For instance, the 2011 August 9 event was associated with a very powerful flare (X6.9) and high-speed CME ($\sim$1610 km s^{-1}). In this event, Gopalswamy et al. (2013) found that the coronal shock was weak and the CME was dim and faint. Thus, the CME speed is relatively less powerful compared to its associated flare strength. However, the CME speed still seems to maintain the proportionality with flare fluence, which is similar to that of some GLEs.

5.2. Remarks on the Four Atypical Non-GLE-SEP Events

Illustrations by several researchers as briefed above (Section 5.1) indicate that the four non-GLEs were exceptional events. As mentioned earlier (Section 4.5), for any exceptional GLE, the ϕ (J m^{-2}) and $V_{\rm cme}$ (km s^{-1}) that do not maintain a near-linear trend over the flare whole phase do maintain at least a minimum rational proportionality over the flare rise phase, whereas this characteristic was not generally observed for non-GLEs. However, the proportional trend between the flare whole phase fluence ϕ_w (J m^{-2}) and $V_{\rm cme}$ (km s^{-1}) of these four non-GLEs being similar to those of some GLEs has raised the possibility of the four non-GLEs being GLEs. The possibility is corroborated by the result in Figure 6, which indicates that the four non-GLE-SEPs occurred before flare prompt and type II onsets, as well as like those of GLE-SEPs nearly at the Sun.

The distinction noticed so far shows that the flares of these four non-GLEs originated from the northern hemisphere, while most of the GLE flares originated from the southern hemisphere. However, a few GLE flares also originated from the northern hemisphere of the Sun (see Tables 1 and 2). This means that there is a possibility that the four non-GLE-SEPs to have grown as GLEs at the Sun, and accordingly, they are supposed to have appeared at the Earth as GLEs ($\geqslant$1 GeV), or at least as sub-GLEs (<1 GeV; e.g., Atwell et al. 2015; Poluianov et al. 2017; Heber et al. 2018).

The disappearance of those possible GLEs or sub-GLEs at the Earth might be interpreted in terms of some arguments. For example, the interplanetary spiral magnetic field is a turbulent complex process controlled by a variety of factors; thus, scatter-free particles are generally not observed, so the particles might undergo a scattering process and energy losses. At times, only a small fraction of the GeV particles generate cascades in the upper atmosphere, as comprehended by seeing the steep energy spectrum of the MeV particles, and thus most of the GeV particles produced in the Sun might not reach the Earth. Furthermore, the particle propagation can be affected by the angular separation between the source on the Sun and observer on the Earth. Severe geomagnetic storms can also affect the particles' access to the Earth. The intensities of the particles undergoing trajectories in the magnetosphere might also vary depending on the transmissivity function (e.g., Shea & Smart 1982; Kudela & Usoskin 2004; Kuznetsov et al. 2005; Kress et al. 2010; Mewaldt et al. 2012; Kurt et al. 2018).

6. General Discussion

The standard flare–CME model (e.g., Aschwanden 2001, 2004; Qiu et al. 2004; Forbes et al. 2006; Aschwanden et al. 2015; Grechnev et al. 2018) illustrates that the thermal/nonthermal and mechanical energy are generally released from the same magnetic reconnection; the released thermal/nonthermal energy manifested in flare components and the mechanical energy manifested in CMEs are thus interrelated (e.g., Hundhausen 1993; Dryer 1994; Cliver et al. 2004; Yihua 2005; Aschwanden 2006, 2017; Miklenic et al. 2009; Liu et al. 2010; Su et al. 2011, 2013; Bein et al. 2012; Grechnev et al. 2013, 2015a). Following the model, we observed (e.g., Figure 1) that the CME acceleration phase and SXR (thermal) flare rise phase evolve almost simultaneously. This supports the previous suggestions that the CME acceleration phases cease over/around the flare peaks and are intimately related to thermal flare components (e.g., Zhang et al. 2002, 2004; Cheng et al. 2003; Li & Zank 2005; Zhang & Dere 2006; Chen & Kunkel 2010; Jang et al. 2017). The intimate relation has been illustrated (Figures 2–4) using the flare fluences (ϕ J m^{-2}) and CME speeds ($V_{\rm cme}$ km s^{-1}).

Spatial evolution of the flare and CME describes how flares originate more or less earlier than the CMEs (e.g., Wang 1993; Jing et al. 2005; Regnier & Priest 2007; Aschwanden 2008; Liu et al. 2009; Firoz et al. 2012, 2017). It is also realized from spectral evolution that the ending phase of the type III burst

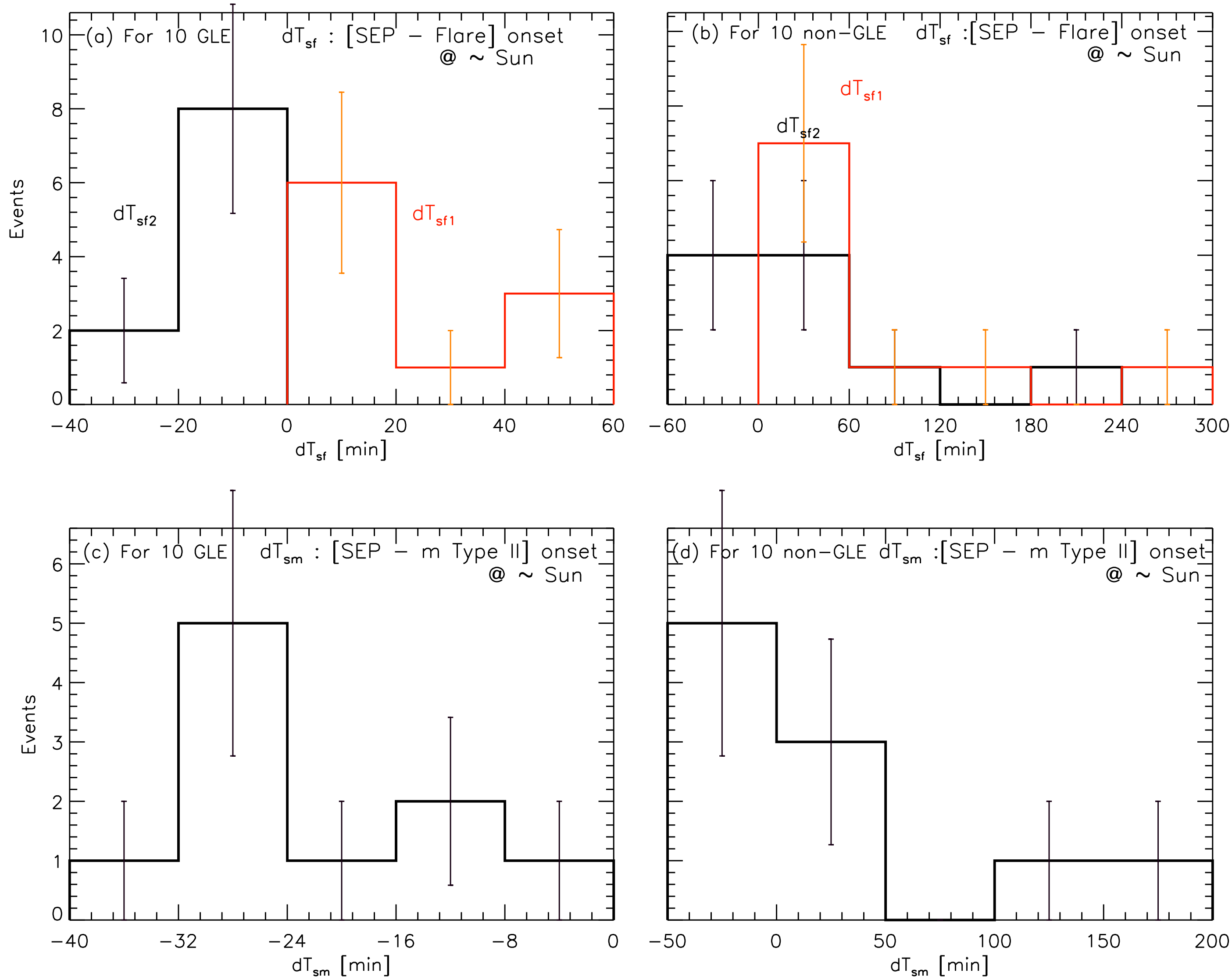

Figure 6. Distributions of injection onset time delays of SEP events and some electromagnetic components during 10 GLE-SEP events and 10 non-GLE-SEP events. (a) and (b) Distribution of the time delay (dT_{sf}) between SEP and flare onset at ∼ the Sun; black histograms represent dT_{sf2} = SEP onset—flare onset2, while red histograms represent dT_{sf1} = SEP onset—flare onset1. (c) and (d) Time delay (dT_{sm}) between SEP and m type II onset. These data are taken from Firoz et al. (2019).

concurring with the flare and the starting phase of the type II burst concurring with CME shocks do coexist (e.g., Firoz et al. 2011b, 2015). Thus, the cause of GLEs depends on the relative importance or/ impact of the two processes (e.g., Cane et al. 2002, 2007; Temmer et al. 2010; Firoz et al. 2015). It was explained by Firoz et al. (2019) that the flare primary phase initiating the MeV particles might exclude the feedback of CME, while the flare prompt phase accelerating the MeV particles to GeV energetics might not exclude the feedback of the CME main acceleration phase, and thus GLE production requires an energy contribution from both the flare and CME acceleration processes.

The distributions (Figures 2–4) of the flare fluences and CME speeds suggest that the correlation magnitude depends on their proportional trends or, in other words, the relative importance or/ impact of the two processes, which might be controlled by the energy released from the magnetic reconnection process (e.g., Bazilevskaya 2008; Grechnev et al. 2008; Liu et al. 2009). When the relative importance of the flare and CME is developed in rational proportionality, it might produce a GLE. This further suggests that a medium or even weak flare and fast CME maintaining rational proportionality may also cause a GLE. This otherwise agrees with the contents of some studies (e.g., Nitta et al. 2012) that even a weak flare and CME might cause a GLE, provided there remains strong magnetic configuration and connectivity to the observer (e.g., Chertok et al. 2013; Luhmann et al. 2018). Thus, the bottom line of this study calls attention to the coronal magnetic field configuration, as the energies released from the magnetic reconnection contain both flare thermal/nonthermal and CME mechanical energy components (e.g., Qiu et al. 2004; Yihua 2005; Aschwanden 2006, 2008; Hudson 2007).

7. Summary and Conclusion

We studied the relationship between flares and CMEs during the SEP events associated with GLEs and during the SEP events with no GLEs. Important results are summarized as follows.

1. This study supports the suggestions of some previous studies that the CME acceleration phases cease around/over flare peaks while being intimately related to the flare impulsive phases (e.g., Figure 1).
2. Most of the data points of flare fluences (J m^{-2}) and CME speeds (km s^{-1}) for GLEs follow a near-linear trend, with the fluences increasing as the CME speeds increase, resulting in a strong positive correlation ($r \geqslant 0.82$), whereas the correlation ($r \leqslant 0.47$) remains weak for non-GLEs. The correlation strength depends on the proportional trend between the flare fluences and CME speeds (e.g., Figure 2).
3. The flare fluences (J m^{-2}) and CME speeds (km s^{-1}) of GLEs that do not maintain a near-linear trend over the flare whole phase do maintain at least a minimum rational proportionality over either the rise or decay phase (e.g., Figures 2 and 3).
4. Flare peak fluences (J m^{-2}) and CME speeds (km s^{-1}) maintain a weak correlation for both GLEs and non-GLEs (e.g., Figure 4), likely because the CME main acceleration ceases over/around the flare peak (e.g., Figure 1).
5. Though the flare peak fluence (J m^{-2}) governs the flare total fluence, it does not blur the correlation magnitude between the flare rise phase and CME speeds (km s^{-1}), thereby indicating that the flare peak fluence or strength does not control the occurrence of GLEs (e.g., Figure 4).
6. The strong or weak correlation depends on the proportional trend between the flare fluences and CME speeds (e.g., Figures 2–5), which are likely related to the conjugation between the flares and CMEs originated from the same magnetic reconnection process.
7. Though the flare fluences (J m^{-2}) and CME speeds (km s^{-1}) of some disparate non-GLE-SEPs show a near-linear trend, they indeed originated over the flare impulsive phase associated with the coronal shock manifested in m type II bursts, whereas GLE-associated SEPs originated over the flare initial phase before the flare prompt and m type II onsets (e.g., Figure 6). Even though a few atypical non-GLE-SEPs originated before the flare prompt and m type II onsets, like those of GLE-SEPs, they did not appear as GLEs at the Earth, presumably because of unfavorable conditions in the interplanetary space as well as the magnetosphere.

The study calls attention to the coronal magnetic field reconnection causing releases of flare thermal/nonthermal energy and CME mechanical energy so as to understand the rational proportionality or relative impact of the flare and CME that seems to be the reason for GLE occurrences.

This work was supported by the BK21 plus program through the National Research Foundation (NRF) funded by the Ministry of Education of Korea. W.Q.G. acknowledges NSFC and CAS grants (U1731241, 11427803, and XDA15052200). J.R.P acknowledges FEDER/Ministerio de Ciencia, Investigación y Universidades/Agencia Estatal de Investigación/Project ESP2017-88436-R. Y.P.L. acknowledges the Joint Research Fund in Astronomy (U1631242) under the cooperative agreement between NSFC and CAS. Some discussions with Professor Victor V. Grechnev (ISTP/RAS) are acknowledged. This article is dedicated to Professor Karel Kudela (IEP/SAS), who made a huge contribution to astrophysics and space science.

ORCID iDs

K. A. Firoz https://orcid.org/0000-0002-1277-1617
Y.-J. Moon https://orcid.org/0000-0001-6216-6944

References

Andriopoulou, M., Mavromichalaki, H., Plainaki, C., Belov, A., & Eroshenko, E. 2011a, SoPh, 269, 155
Andriopoulou, M., Mavromichalaki, H., Preka-Papadema, P., Belov, A., & Eroshenko, E. 2011b, ASTRA, 7, 439
Andriopoulou, M., Plainaki, C., Mavromichalaki, H., Belov, A., & Eroshenko, E. 2009, 21st European Cosmic Ray Symp., ed. P. Kiraly (Košice: Institute of Experimental Physics), 254
Aschwanden, M. J. 2001, ApJ, 560, 1035
Aschwanden, M. J. 2002, SSRv, 101, 1
Aschwanden, M. J. 2004, ApJ, 608, 554
Aschwanden, M. J. 2006, SSRv, 124, 361
Aschwanden, M. J. 2012, SSRv, 171, 3
Aschwanden, M. J. 2017, ApJ, 847, 27
Aschwanden, M. J., & Freeland, S. L. 2012, ApJ, 754, 112
Aschwanden, M. J., Schrijver, C. J., & Malanushenko, A. 2015, SoPh, 290, 2765
Aschwanden, M. J. 2008, in ASP Conf. Ser. 383, 24th Int. NSO/SP Workshop Subsurface & Atmospheric Influences on Solar Activity, ed. R. Howe et al. (San Francisco, CA: ASP), 1
Asvestari, E., Willamo, T., Gil, A., et al. 2017, AdSpR, 60, 781
Atwell, W., Tylka, A. J., Dietrich, W., Rojdev, K., & Marzkind, C. 2015, in 45th Int. Conf. on Environment Systems, (Houston, TX: Paragon Space Development Corp.), 20150009484, https://ntrs.nasa.gov/search.jsp?R=20150009484
Baisultanova, L. M., Belov, A. V., Dorman, L. I., et al. 1991, Proc. ICRC (Dublin), 22, 105
Battarbee, M., Guo, J., Dalla, S., et al. 2018, A&A, 612, A116
Bazilevskaya, G. A. 2008, AdSpR, 43, 530
Bein, B. M., Berkebile-Stoiser, S., Veronig, A. M., Temmer, M., & Vršnak, B. 2012, ApJ, 755, 44
Belov, A., Garcia, H., Kurt, V., Mavromichalaki, H., & Gerontidou, M. 2005, SoPh, 229, 135
Belov, A. V., & Eroshenko, E. A. 1996, RadM, 26, 461
Belov, A. V., Eroshenko, E. A., Kryakunova, O., et al. 2015, JPhCS, 632, 012063
Belov, A. V., Eroshenko, E. A., Kryakunova, O. N., Kurt, V. G., & Yanke, V. G. 2010, Ge&Ae, 50, 21
Belov, A. V., & Struminsky, A. B. 2017, BRASP, 81, 124
Bieber, J. W., Clem, J., Evenson, P., et al. 2013, ApJ, 771, 92
Bieber, J. W., Clem, J. M., Duldig, M. L., et al. 2004, JGR, 109, A12106
Bombardieri, D. J., Duldig, M. L., Humble, J. E., & Michael, K. J. 2008, ApJ, 682, 1315
Brueckner, G. E., Howard, R. A., Koomen, M. J., et al. 1995, Sol Phys, 162, 357
Bütikofer, R., Flückiger, E. O., Desorgher, L., Moser, M. R., & Pirard, B. 2009, AdSpR, 43, 499
Cane, H. V., Erickson, W. C., & Prestage, N. P. 2002, JGRA, 107, 1315
Cane, H. V., Richardson, I. G., & von Rosenvinge, T. T. 2007, SSRv, 130, 301
Cane, H. V., von Rosenvinge, T. T., Cohen, C. M. S., & Mewaldt, R. A. 2003, GeoRL, 30, 8017
Chandra, R., & Uddin, W. 2006, SunGe, 1, 42
Chen, J., & Kunkel, V. 2010, ApJ, 717, 1105
Cheng, C. Z., Ren, Y., Choe, G. S., & Moon, Y.-J. 2003, ApJ, 596, 1341
Chertok, I. M., Grechnev, V. V., Below, A. V., & Abunin, A. A. 2013, SoPh, 282, 175
Chupp, E. L., & Ryan, J. M. 2009, RAA, 9, 11
Clem, J. M., & Dorman, L. I. 2000, SSRv, 93, 335
Cliver, E. W., Kahler, S. W., Cane, H. V., et al. 1983, SoPh, 89, 181
Cliver, E. W., Kahler, S. W., & Reames, D. V. 2004, ApJ, 605, 902
Cliver, E. W., Kahler, S. W., Shea, M. A., & Smart, D. F. 1982, ApJ, 260, 362
Cliver, E. W., Laurenza, M., Storini, M., & Thompson, B. J. 2005, ApJ, 631, 604
Cliver, E. W. 2006, ApJ, 639, 1206
Cochran, W. G. 1952, The Annals of Mathematical Statistics, 23, 315
Cramp, J. L., Duldig, M. L., Fluckiger, E. O., et al. 1997, JGR, 102, 24237

Cyr, O. C., St., Plunkett, S. P., Michels, D. J., et al. 2000, JGR, 105, 18169
Dayeh, M. A., Desai, M. I., Kozarev, K., et al. 2010, SpWea, 8, S00E07
Debrunner, H., Flueckiger, E. O., & Lockwood, J. A. 1990, ApJS, 73, 259
Deeley, K. M., Duldig, M. L., & Humble, J. E. 2002, AdSpR, 30, 1049
Delaboudiniere, J.-P., Artzner, G. E., Brunaud, J., et al. 1995, SoPh, 162, 91
Dierckxsens, M., Tziotziou, K., Dalla, S., et al. 2015, SoPh, 290, 841
Domingo, V., Fleck, B., & Poland, A. I. 1995, SSRv, 72, 81
Dryer, M. 1994, in Proc. 3rd SOHO Workshop, ESA SP-373, ed. J. J. Hunt (Noordwijk: ESA), 101
Duldig, M. L. 1999, Proc. ICRC (Salt Lake City), 26, 403
Duldig, M. L. 2001, Proc. ICRC (Hamburg), 27, 3363
Duldig, M. L., Cramp, J. L., Humble, J. E., et al. 1993, PASAu, 10, 211
El-Borie, M. A. 2003, APh, 19, 549
Emslie, A. G., Dennis, B. R., Shih, A. Y., et al. 2012, ApJ, 759, 71
Firoz, K. A., Cho, K.-S., Hwang, J., et al. 2010, JGR, 115, A09105
Firoz, K. A., Gan, W. Q., Li, Y. P., et al. 2014b, ApJS, 213, 24
Firoz, K. A., Gan, W. Q., Li, Y. P., & Rodríguez-Pacheco, J. 2014a, Ap&SS, 250, 21
Firoz, K. A., Gan, W. Q., Li, Y. P., & Rodriguez-Pacheco, J. 2015, SoPh, 290, 613
Firoz, K. A., Gan, W. Q., Li, Y. P., Rodríguez-Pacheco, J., & Kudela, K. 2019, ApJ, 872, 178
Firoz, K. A., Gan, W. Q., Li, Y. P., Rodríguez-Pacheco, J., & Su, Y. 2017, Ap&SS, 362, 113
Firoz, K. A., Gan, W. Q., Moon, Y.-J., & Li, C. 2012, ApJ, 758, 119
Firoz, K. A., Hwang, J., Dorotovič, I., Pintér, T., & Kaushik, S. C. 2011a, Ap&SS, 331, 469
Firoz, K. A., Moon, Y.-J., Moon, Y. J., et al. 2011b, ApJ, 743, 190
Forbes, T. G., Linker, J. A., Chen, J., et al. 2006, SSRv, 123, 251
Fujimoto, K., Kojima, H., & Murakami, K. 1985, ICRC, 19, 262
Gopalswamy, N., Akiyama, S., Yashiro, S., et al. 2014, GeoRL, 41, 2673
Gopalswamy, N., Xie, H., Akiyama, S., et al. 2013, ApJL, 765, L30
Gopalswamy, N., Xie, H., Yashiro, S., & Usoskin, I. 2005, ICRC (Pune), 29, 101
Gopalswamy, N., Yashiro, S., Krucker, S., Stenborg, G., & Howard, R. A. 2004, JGR, 109, A12105
Grechnev, V., Kurt, V. G., Chertok, I. M., et al. 2008, SoPh, 252, 149
Grechnev, V., Uralov, A. M., Kiselev, V. I., & Kochanov, A. A. 2017, SoPh, 292, 3
Grechnev, V. V., Kiselev, V. I., Kashapova, L. K., et al. 2018, SoPh, 293, 133
Grechnev, V. V., Kiselev, V. I., Meshalkina, N. S., & Chertok, I. M. 2015a, SoPh, 290, 2827
Grechnev, V. V., Kiselev, V. I., Meshalkina, N. S., & Chertok, I. M. 2015b, SoPh, 290, 10
Grechnev, V. V., Kiselev, V. I., Uralov, A. M., Meshalkina, N. S., & Kochanov, A. A. 2013, PASJ, 65, S9
Grechnev, V. V., & Kochanov, A. A. 2016, SoPh, 291, 12
Haider, S. A., McKenna-Lawlor, S. M. P., Fry, C. D., Jain, R., & Joshipura, K. N. 2012, JGR, 117, A05326
Hanuise, C., Cerisier, J. C., Auchère, F., et al. 2006, AnGeo, 24, 129
Harrison, R. A. 1995, A&A, 304, 585
Heber, B., Augeda, N., Bütikofer, R., et al. 2018, in Solar Particle Radiation Storms Forecasting and Analysis, ed. O. E. Malandraki & N. B. Crosby (Cham: Springer), 179
Hofer, M. Y., & Storini, M. 2001, MmSAI, 72, 624
Howard, R. A., Moses, J. D., Vourlidas, A., et al. 2008, SSRv, 136, 67
Hu, H., Liu, Y. D., Wang, R., Möstl, C., & Yang, Z. 2016, ApJ, 829, 97
Hu, S., Kim, M. Y., McClellan, G., & Cucinotta, F. A. 2009, HeaPh, 96, 465
Hudson, H. S. 2007, in ASP Conf. Ser. 368, The Physics of Chromospheric Plasmas, ed. P. Heinzel, I. Dorotoviè, & R. J. Rutten (San Francisco, CA: ASP), 365
Hundhausen, A. J. 1993, JGR, 98, 13177
Hundhausen, A. J. 1999, in The Many Faces of the Sun: A Summary of the Results from NASA's Solar Maximum Mission, ed. T. S. Keith et al. (New York: Springer), 143
Jang, S., Moon, Y.-J., Kim, R.-S., Kim, S., & Lee, J.-O. 2017, ApJ, 845, 169
Jing, J., Qiu, J., Lin, J., et al. 2005, ApJ, 620, 1085
Kahler, S. W. 1994, ApJ, 428, 837
Kahler, S. W., Reames, D. V., & Sheeley, N. R., Jr. 2001, ApJ, 562, 558
Kahler, S. W., Sheeley, N. R., Jr., & Liggett, M. 1989, ApJ, 344, 1026
Kahler, S. W., & Vourlidas, A. 2005, JGRA, 110, A12S01
King, J. H., & Papitashvili, N. E. 2005, JGR, 110, A02104
Klassen, A., Aurass, H., Klein, K.-L., Hofmann, A., & Mann, G. 1999, A&A, 343, 287
Klassen, A., Bothmer, V., Mann, G., et al. 2002, A&A, 385, 1078
Kress, B. T., Mertens, C. J., & Wiltberger, M. 2010, SpWea, 8, S05001
Krucker, S., & Benz, A. O. 1998, ApJL, 501, L213
Kudela, K. 1990, ApJS, 73, 297
Kudela, K., & Langer, R. 2005, CoSka, 25, 5
Kudela, K., Shea, M. A., Smart, D. F., & Gentile, L. C. 1993, Proc. ICRC (Singapore), 23, 71
Kudela, K., & Usoskin, I. G. 2004, CzJPh, 54, 239
Kudela, K., Venkatesan, D., Flueckiger, E. O., et al. 1995, ICRC (Rome), 24, 928
Kühl, P., Banjac, S., Dressing, N., et al. 2015, A&A, 576, A120
Kurt, V., Belov, A., Kudela, K., & Yushkov, B. 2018, CoSka, 48, 329
Kurt, V., Belov, A., Mavromichalaki, H., & Gerontidou, M. 2004, AnGeo, 22, 2255
Kurt, V., Yushkov, B., Belov, A., Chertok, I., & Grechnev, V. 2013, JPhCS, 409, 012151
Kurt, V. G., Yushkov, B. Y., & Belov, A. 2010, AstL, 36, 520
Kuwabara, T., Bieber, J. W., Clem, J., Evenson, P., & Pyle, R. 2006, SpWea, 4, S10001
Kuznetsov, S. N., Kudela, K., Bucik, R., & Yushkov, B. Y. 2005, ICRC (Pune), 29, 409
Kuznetsov, S. N., Kurt, V. G., Yushkov, B. Y., et al. 2006, CoSka, 36, 85
Li, G., & Zank, G. P. 2005, GeoRL, 32, L02101
Li, Y. P., Feng, L., Zhang, P., Liu, S. M., & Gan, W. Q. 2016, RAA, 16, 161
Liu, C., Lee, J., Karlickímath, M., et al. 2009, ApJ, 703, 757
Liu, Y., Thernisien, A., Luhmann, J. G., et al. 2010, ApJ, 722, 1762
Lovell, J. L., Duldig, M. L., & Humble, J. E. 1998, JGR, 103, 23733
Low, B. C. 1996, SoPh, 167, 217
Luhmann, J. G., Mays, M. L., Li, Y., et al. 2018, SpWea, 16, 557
Makhmutov, V. S., Stozhkov, Y. I., Bazilevskaya, G. A., Svirzhevsky, N. S., & Morzabayev, A. K. 2009, Bulletin of the Russian Academy of Sciences: Physics, 73, 350
Maurchev, E. A, Balabin, Y. V., Vashenyuk, E. V., & Gvozdevsky, B. B. 2013, JPhCS, 409, 012200
Maričić, D., Vršnak, B., Stanger, A. L., et al. 2007, SoPh, 241, 99
Mavromichalaki, H., Papaioannou, A., Gerontidou, M., et al. 2013, JPhCS, 409, 012206
Mavromichalaki, H., Papaioannou, A., Plainaki, C., Sarlanis, C., et al. 2011, AdSpR, 47, 2210
Mavromichalaki, H., Papaioannou, A., Mariatos, G., et al. 2007, ITNS, 54, 1089
Mavromichalaki, H., Souvatzoglou, G., Sarlanis, C., et al. 2006, AdSpR, 37, 1141
Mavromichalaki, H., Souvatzoglou, G., Sarlanis, C., et al. 2010, NewA, 15, 744
Mewaldt, R. A., Looper, M. D., Cohen, C. M. S., et al. 2012, SSRv, 171, 97
Miklenic, C. H., Veronig, A. M., & Vršnak, B. 2009, A&A, 499, 893
Mironova, I. A., Aplin, K. L., Arnold, F., et al. 2015, SSRv, 194, 1
Miroshnichenko, L. I., Vashenyuk, E. V., & Pérez-Peraza, J. A. 2013, Ge&Ae, 53, 541
Mishev, A., & Usoskin, I. 2016, SoPh, 291, 1225
Mishev, A., Usoskin, I., & Kocharov, L. 2017, ICRC (Busan), 35, 147
Mishev, A., Usoskin, I., Raukunen, O., et al. 2018, SoPh, 293, 136
Moon, Y.-J., Choe, G. S., Wang, H., et al. 2002, ApJ, 581, 694
Moore, D. S. 2006, Basic Practice of Statistics (4th ed.; New York: Freeman)
Muraki, Y., Matsubara, Y., Masuda, S., et al. 2008, APh, 29, 229
Nagashima, K., Fujimoto, K., & Sakakibara, S. 1992, P&SS, 40, 1109
Ning, Z., Ding, M. D., Qiu, K. P., et al. 2008, Ap&SS, 315, 45
Ning, Z., Fang, C., Ding, M. D., et al. 2005, in IAU Symp. 226, Coronal and Stellar Mass Ejections, ed. K. Dere, J. Wang, & Y. Yan (Cambridge: Cambridge Univ. Press), 123
Nitta, N. V., Cliver, E. W., & Tylka, A. J. 2003, ApJL, 586, L103
Nitta, N. V., Liu, Y., DeRosa, M. L., & Nightingale, R. W. 2012, SSRv, 171, 61
Núñez, M. 2011, SpWea, 9, S07003
Papaioannou, A., Anastasiadis, A., Kouloumvakos, A., et al. 2018, SoPh, 293, 23
Papaioannou, A., Belov, A., Mavromichalaki, H., Eroshenko, E., & Oleneva, V. 2009, AdSpR, 43, 582
Papaioannou, A., Sandberg, I., Anastasiadis, A., et al. 2016, JSWSC, 6, A42
Papaioannou, A., Souvatzoglou, G., Paschalis, P., Gerontidou, M., & Mavromichalaki, H. 2014, SoPh, 289, 423
Pérez-Peraza, J., Gallegos-Cruz, A., Vashenyuk, E. V., Balaban, E., & Miroshnichenko, L. I. 2006, AdSpR, 38, 418
Pérez-Peraza, J., & Juárez-Zuñiga, A. 2015, ApJ, 803, 27
Pérez-Peraza, J., Márquez-Adame, J. C., Miroshnichenko, L., & Velasco-Herrera, V. 2018, JGRA, 123, 3262
Plainaki, C., Belov, A., Eroshenko, E., et al. 2005, AdSpR, 35, 691

Plainaki, C., Belov, A., Eroshenko, E., Mavromichalaki, H., & Yanke, V. 2007, JGRA, 112, A04102
Pohjolainen, S., Al-Hamadani, F., & Valtonen, E. 2015, ICRC (The Hague), 34, 86
Poluianov, S., Usoskin, I., Mishev, A., Shea, M., & Smart, D. 2017, SoPh, 292, 176
Qiu, J., Wang, H., Cheng, C. Z., & Gary, D. E. 2004, ApJ, 604, 900
Raukunen, O., Vainio, R., Tylka, A. J., et al. 2018, JSWSC, 8, A04
Reames, D. V. 1999, SSRv, 90, 413
Reames, D. V. 2009, ApJ, 706, 844
Regnier, S., & Priest, E. R. 2007, A&A, 468, 701
Ruffolo, D., Matthaeus, W. H., & Chuychai, P. 2003, ApJL, 597, L169
Ryabko, B. Ya., Stognienko, V. S., & Shokin, Yu. I. 2004, Journal of Statistical Planning and Inference, 123, 365
Sabbah, I. 2000, CaJPh, 78, 293
Sáiz, A., Ruffolo, D., Rujiwarodom, M., et al. 2005, ICRC (Pune), 29, 229
Salas-Matamoros, C., & Klein, K.-L. 2015, SoPh, 290, 1337
Schwenn, R., Inhester, B., Plunkett, S. P., et al. 1997, SoPh, 175, 667
Shea, M. A., & Smart, D. F. 1982, SSRv, 32, 251
Shea, M. A., & Smart, D. F. 1996, AIP Conf. Proc., 374 High energy solar physics (Melville, NY: AIP), 131
Shea, M. A., & Smart, D. F. 2012, SSRv, 171, 161
Shea, M. A., Smart, D. F., Humble, J. E., et al. 1987, ICRC (Moscow), 20, 171
Shen, C., Li, G., Kong, X., Hu, J., et al. 2013, ApJ, 763, 114
Simnett, G. M. 2006, A&A, 445, 715
Simnett, G. M. 2007, A&A, 472, 309
Smart, D. F., Shea, M. A., & Taskanen, P. J. 1971, ICRC (Tasmania), 12, 483
Souvatzoglou, G., Papaioannou, A., Mavromichalaki, H., Dimitroulakos, J., & Sarlanis, C. 2014, SpWea, 12, 633
Storini, M., Kudela, K., Cordaro, E. G., & Massetti, S. 2005, AdSpR, 35, 416
Struminsky, A. B. 2005, ICRC, 1, 45
Su, Y., Holman, G. D., & Dennis, B. R. 2011, ApJ, 731, 106
Su, Y., Veronig, A. M., Holman, G. D., et al. 2013, NatPh, 9, 489
Takasaki, H., Asai, A., Kiyohara, J., et al. 2004, ApJ, 613, 592
Temmer, M., Veronig, A. M., Kontar, E. P., Krucker, S., & Vrsnak, B. 2010, ApJ, 712, 1410
Thakur, N., Gopalswamy, N., Makela, P., et al. 2016, SoPh, 291, 513
Thernisien, A., Vourlidas, A., & Howard, R. A. 2009, SoPh, 256, 111
Tylka, A. J., Boberg, P. R., Cohen, C. M. S., et al. 2002, ApJL, 581, L119
Tylka, A. J., Cohen, C. M. S., Dietrich, W. F., et al. 2005, ApJ, 625, 474
Usoskin, I. G., Mursula, K., & Kangas, J. 2001, ICRC (Hamburg), 27, 3842
Vashenyuk, E. V., Balabin, Y. V., Germanenko, A. V., & Gvozdevsky, B. B. 2011, ASTRA, 7, 453
Vashenyuk, E. V., Balabin, Y. V., & Gvozdevsky, B. B. 2003, ICRC (Lodz), 28, 3401
Vashenyuk, E. V., Balabin, Y. V., Gvozdevsky, B. B., & Karpov, S. N. 2006, Ge&Ae, 46, 424
Vashenyuk, E. V., Fischer, S., & Gvozdevsky, B. B. 1993, ICRC (Singapore), 23, 266
Vashenyuk, E. V., Miroshnichenko, L. I., Perez-Peraza, J., et al. 1997, Proc. ICRC (Durban, South Africa), 1, 161
Vashenyuk, E. V., Miroshnichenko, L. I., Sorokin, M. O., Peŕez-Peraza, J., & Gallegos-Cruz, A. 1994, AdSpR, 14, 711
Velinov, P. I. Y., & Mishev, A. 2013, JPhCS, 409, 012211
Veronig, A., Vršnak, B., Dennis, B. R., et al. 2002, A&A, 392, 699
Vršnak, B., Sudar, D., & Ruždjak, D. 2005, A&A, 435, 1149
Wang, H. 1993, SoPh, 140, 85
Wang, R., Liu, Y. D., Thomas, W., et al. 2016, SoPh, 291, 1159
Wu, S.-S., & Qin, G. 2017, JGRA, 123, 76
Yashiro, S., & Gopalswamy, N. 2009, in IAU Symp. 257, Universal Heliophysical Processes, ed. N. Gopalswamy & D. F. Webb (Cambridge: Cambridge Univ. Press), 233
Yihua, Y. 2005, SSRv, 121, 213
Zhang, J., & Dere, K. P. 2006, ApJ, 649, 1100
Zhang, J., Dere, K. P., Howard, R. A., Kundu, M. R., & White, S. M. 2001, ApJ, 559, 452
Zhang, J., Dere, K. P., Howard, R. A., & Vourlidas, A. 2004, ApJ, 604, 420
Zhang, M., Golub, L., DeLuca, E., & Burkepile, J. 2002, ApJL, 574, L97
Zucca, P., Núñez, M., & Klein, K. 2017, JSWSC, 7, A13